Photomagnetic K(0.25)Ni(1-x)Co(x)[Fe(CN)6]·nH2O and K(0.25)Co[Fe(CN)6](0.75y)[Cr(CN)6](0.75(1-y))·nH2O Prussian blue analogue solid solutions.

ARTICLE *in* INORGANIC CHEMISTRY · MARCH 2012

Impact Factor: 4.76 · DOI: 10.1021/ic202571d · Source: PubMed

3 AUTHORS, INCLUDING:

Takashi Yamamoto
Keio University
24 PUBLICATIONS **329** CITATIONS

SEE PROFILE

Inorganic Chemistry

Article

pubs.acs.org/IC

Photomagnetic $K_{0.25}Ni_{1-x}Co_x[Fe(CN)_6]\cdot nH_2O$ and $K_{0.25}Co[Fe(CN)_6]_{0.75y}[Cr(CN)_6]_{0.75(1-y)}\cdot nH_2O$ Prussian Blue Analogue Solid Solutions

Daniel M. Pajerowski,*[,†,‡] Takashi Yamamoto,[‡] and Yasuaki Einaga*[,‡]

[†]NIST Center for Neutron Research, Gaithersburg, Maryland 20899, United States

[‡]Department of Chemistry, Keio University, 3-14-1 Hiyoshi, Yokohama 223-8522, Japan

ABSTRACT: Magnetically bistable solid solutions of Prussian blue analogues with chemical formulas of $K_\alpha Ni_{1-x}Co_x[Fe(CN)_6]_\beta\cdot nH_2O$ ($Ni_{1-x}Co_xFe$) and $K_\alpha Co_\gamma[Fe(CN)_6]_y[Cr(CN)_6]_{1-y}\cdot nH_2O$ ($CoFe_yCr_{1-y}$) have been synthesized and studied using mass spectrometry, Mössbauer spectroscopy, X-ray diffraction, temperature-dependent infrared spectroscopy, and dc magnetometry. These compounds provide insight into interfaces between the photomagnetic Co−Fe Prussian blue analogue and the high-T_C Ni−Cr Prussian blue analogue that exist in high-T_C photomagnetic heterostructures. This investigation shows that the bistability of Co−Fe is strongly modified by metal substitution, with $Ni_{1-x}Co_xFe$ stabilizing high-spin cobalt−iron pairs and $CoFe_yCr_{1-y}$ stabilizing low-spin cobalt−iron pairs, while both types of substitution cause a dramatic decrease in the bistability of the material.

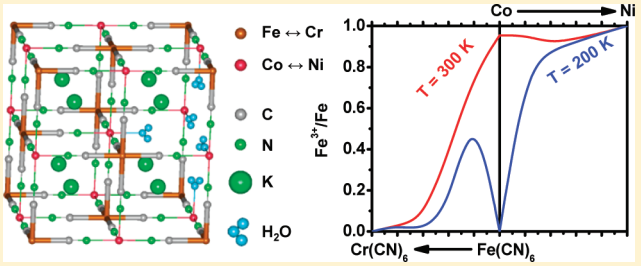

I. INTRODUCTION

Photocontrol of magnetic materials is an exciting field of research because of the strong potential for device application, and new photomagnetic materials are brought to light each year. To date, an assortment of photomagnetic materials exist in the published literature,[1−3] including magnetic semiconductors with organic constituents,[4−6] spin-crossover materials,[7,8] and charge transfer induced spin transition (CTIST) compounds.[9−11] Recently, high-T_C photocontrol of long-range magnetic order in heterostructures of cobalt hexacyanoferrate and nickel hexacyanochromate Prussian blue analogues (PBAs) has been reported.[12−14] These heterostructures display an intriguing new type of photoeffect that is due to interlayer interactions of the "meta-material" on the nanoscale and will require additional study to be well understood.

Prussian blue is the canonical cubic complex-cyanide compound, and PBAs are materials isostructural to Prussian blue with the more general chemical formula of $A_jM1_k[M2(CN_6)]_l nH_2O$ (henceforth M1−M2), where A is an interstitial cation and M1 and M2 are networked metal ions.[15] The Prussian blue lattice is classified as a member of space group $Fm\bar{3}m$ (No. 225) and consists of M1 and M2 ions octahedrally coordinated by nitrogen and carbon, respectively, and bridged by cyanides. Higher order structural considerations include interstitial water molecules and $M2(CN)_6$ vacancies coordinated by water molecules.[16] Prussian blue analogues have been the subject of intense study because of their multitude of magnetic effects.[15] Two specifically relevant analogues are Ni−Cr, which displays magnetic order at temperatures up to 90 K,[17] and Co−Fe, which was shown to display photoinduced modification of long-range magnetic order below ∼18 K.[18] Briefly, Co−Fe shows CTIST as a result of either photoirradiation or changes in temperature, and changes in magnetization are due to the transformation of magnetic Co^{2+}−NC−Fe^{3+} pairs to diamagnetic Co^{3+}−NC−Fe^{2+} pairs and vice versa.[10,11,18,19]

In magnets consisting of individual Ni−Cr and Co−Fe layers that are in intimate contact, regions may exist where the two materials are intermixed.[20] An approximation of these mixed regions that may be studied in detail is solid solutions that intermix Ni−Cr and Co−Fe, and the relevant ternary metal solid solutions are $K_\alpha Ni_{1-x}Co_x[Fe(CN)_6]_\beta\cdot nH_2O$ ($Ni_{1-x}Co_xFe$) and $K_\alpha Co_\gamma[Fe(CN)_6]_y[Cr(CN)_6]_{1-y}\cdot nH_2O$ ($CoFe_yCr_{1-y}$). Solid solutions $Ni_{1-x}Co_xFe$ and $CoFe_yCr_{1-y}$ can be thought of as a statistical mixture of interpenetrating PBA lattices, shown in Figure 1. Solid solutions of PBAs have already been studied in detail,[21−32] and there have even been reports on $Ni_{1-x}Co_xFe$.[22,23] However, previous reports were not interested in the particular problem of how CTIST in Co−Fe would be affected by contact and mixing with Ni−Cr.

In the present work, a further investigation of $Ni_{1-x}Co_xFe$ materials is made, with new data specifically related to the question of the bistability of cobalt−iron pairs in a mixed system. In addition, $CoFe_yCr_{1-y}$ samples are presented for the first time with similar attention to how CTIST is modified as a result of the intermixing of materials. Samples are studied using mass spectrometry to determine atomic concentration, Mössbauer spectroscopy to determine iron oxidation states, X-ray diffraction to show the crystal structure, temperature dependent infrared spectroscopy that directly measures the amount of material undergoing CTIST, and dc magnetometry to investigate photo-induced magnetization and quenched magnetic states. The main result of our studies is that the bistability of Co−Fe is strongly

Received: November 29, 2011
Published: March 7, 2012

   dx.doi.org/10.1021/ic202571d | *Inorg. Chem.* 2012, 51, 3648−3655

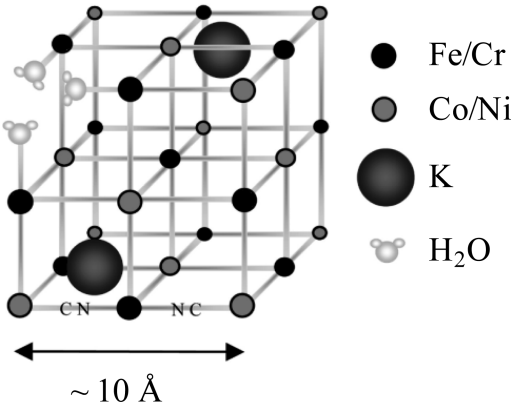

Figure 1. Structure of substitutional solid Prussian blue analogues, $Ni_{1-x}Co_xFe$ and $CoFe_yCr_{1-y}$.

modified by metal substitution, with $Ni_{1-x}Co_xFe$ stabilizing magnetic $Co^{2+}-NC-Fe^{3+}$ pairs and $CoFe_yCr_{1-y}$ stabilizing diamagnetic $Co^{3+}-NC-Fe^{2+}$ pairs.

II. EXPERIMENTAL DETAILS[33]

A. Synthesis. Prussian blue analogues $K_\alpha Ni_{1-x}Co_x[Fe(CN)_6]_\beta \cdot nH_2O$ were precipitated by the dropwise addition of a 200 mL aqueous solution of $Co(NO_3)_2 \cdot 6H_2O$ and $Ni(NO_3)_2 \cdot 6H_2O$ (5×10^{-3} mol/L total in transition metal) to a combination of 50 mL of 2×10^{-2} mol/L $K_3Fe(CN)_6$ and 50 mL of 1×10^{-1} mol/L KNO_3, over the course of several hours. The concentration of cobalt in $Ni_{1-x}Co_xFe$ is given by "x" and is controlled during synthesis by varying the cobalt fraction of the transition metal concentration in solution, defined as $x_{synthesis} = [Co_{(aq)}]/([Co_{(aq)}] + [Ni_{(aq)}])$, while keeping the total transition metal ion concentration at 5×10^{-3} mol/L. Prussian blue analogues $K_\alpha Co_y[Fe(CN)_6]_y[Cr(CN)_6]_{1-y} \cdot nH_2O$ were synthesized in a similar manner, by the dropwise addition of a 200 mL aqueous solution of 5×10^{-3} mol/L $Co(NO_3)_2 \cdot 6H_2O$ to a combination of 50 mL of $K_3Fe(CN)_6$ and $K_3Cr(CN)_6$ (2×10^{-2} mol/L total in transition metal) and 50 mL of 1×10^{-1} mol/L KNO_3, over the course of several hours. The concentration of hexacyanoferrate in $CoFe_yCr_{1-y}$ is given by "y" and is controlled during synthesis by varying the hexacyanoferrate fraction of the hexacyanometalate concentration in solution, defined as $y_{synthesis} = [Fe(CN)_{6(aq)}]/([Fe(CN)_{6(aq)}] + [Cr(CN)_{6(aq)}])$, while keeping the total hexacyanometalate concentration at 2×10^{-2} mol/L. After addition, reaction mixtures were stirred for 3 h in an open atmosphere, and the microcrystalline powders were then isolated by centrifugation. The precipitates were rinsed three times with water and dried under vacuum conditions. Values of $x_{synthesis}$ = 0.00, 0.20, 0.40, 0.60, 0.80, and 1.00 yielded compounds with $x \sim$ 0.00, 0.20, 0.40, 0.60, 0.80, and 1.00, respectively, and values of $y_{synthesis}$ = 0.00, 0.20, 0.40, 0.60, 0.80, and 1.00 yielded compounds with $y \sim$ 0.00, 0.20, 0.40, 0.60, 0.80, and 1.00, respectively. Deionized water of at least 18 MΩ resistivity was used for synthesis. All other reagents were purchased from Wako Pure Chemical Industries, Ltd. and used without further purification.

B. Instrumentation. Mass spectrometry to ascertain metal concentration (K, Ni, Co, Fe, and Cr) and combustion analysis of organic constituents (C, H, and N) was performed by Complete Analysis Laboratories, Inc. (www.calilabs.com). Powder X-ray diffraction (XRD) was performed on a Bruker Advanced X-ray Solutions D8 ADVANCE X-ray diffractometer with a Cu Kα source (λ = 1.5418 A). Mössbauer spectroscopy was performed using a Topologic Systems model 222 constant-acceleration spectrometer with a ^{57}Co/Rh source in transmission mode. Temperature-dependent infrared (IR) spectroscopy was performed on a JASCO FT-IR 660Plus spectrometer and a variable temperature Displex insert. Magnetic measurements were performed using a Quantum Design MPMS XL superconducting quantum interference device (SQUID) magnetometer. A room temperature halogen light source (~1–2 mW) was used to introduce light into the sample chamber of the SQUID through a quartz optical fiber for photomagnetic measurements.

C. Analysis Preparations. For XRD, roughly 100 mg of sample were mounted on flat plastic sample holders. For Mössbauer spectroscopy, between 30 and 50 mg of sample was mounted in cylindrical aluminum sample holders using cellophane tape. Infrared spectroscopy samples were prepared by depositing drops of the final solution from synthesis on CaF_2 slides and drying them under vacuum conditions. For SQUID measurements, samples of roughly 35 mg were mounted in gelcaps, except for photomagnetic measurements in which approximately 1 mg of powder was mounted on clear cellophane tape to increase the light cross-section.

III. RESULTS

A. Elemental Analysis. A chemical formula is proposed for each compound, taking into account the mass fraction of each element, charge balance of the structure, and the chemistry of these systems. The experimental uncertainties of the metal content are estimated to be near a mass fraction of 2%, and the experimental uncertainties of the organic content are estimated to be near a mass fraction of 0.1%, and these uncertainties are considered when calculating the chemical formula. In addition, the procedure utilized for extracting chemical formulas from the elemental analysis also utilized both soft and hard constraints. For example, the abundance of metals on M2 sites is directly related to the amount of C and N in the sample, which was detected with higher precision. Table 1 reports the experimental and proposed mass fraction compositions of the compounds along with a proposed chemical formula, and Figure 2 displays these data. Chemical formulas are normalized to the divalent metal position, and two types of water are delineated, interstitial water and that rounding out the coordination sphere of the divalent site. The oxygen content was not directly measured, but for comparison, a calculation based upon measured hydrogen content is reported. As such, aspects of the proposed chemical formulas may have different mass fractions than the raw elemental analysis data, but the discrepancies are as expected from the characterized experimental uncertainties. Likewise, the global fitting of chemical formulas was chosen for tidiness after independent fits yielded indistinguishable results within experimental uncertainties. More explicit examination of oxidation states' role in chemical formula determination takes place in the Discussion section.

B. Mössbauer Spectroscopy. Because ferricyanide and ferrocyanide may both be present in the PBA lattice, room temperature Mössbauer spectra were recorded for all compounds containing iron, Figure 3. Experimental data are fit using a wider doublet attributed to magnetic, S = 1/2, trivalent iron ions and a narrower doublet that is attributed to diamagnetic divalent iron ions. The doublets are parametrized with an isomer shift (IS), quadrapole splitting (QS), line-width (W), and percent. The results of the fitting procedure are shown in Table 2, and the parameters obtained fall within the range of reported values for similar PBA materials.[34−36] It is interesting that the evolution of the Mössbauer spectra is different for $Ni_{1-x}Co_xFe$ and $CoFe_yCr_{1-y}$ as substitution away from pure CoFe takes place. The results from $Ni_{1-x}Co_xFe$ measurements are consonant with previous reports on similar $Ni_{1-x}Co_xFe$ samples, with most iron being trivalent, a small fraction being divalent, and similar average iron oxidation for all values of x.[22] This behavior is contrasted in the $CoFe_yCr_{1-y}$ data, where increasing chromium substitution stabilizes divalent iron at the expense of trivalent iron.

C. X-Ray Powder Diffraction. X-ray powder diffraction was performed at room temperature and confirmed the PBA crystal structure in all compounds, Figure 4a. However, further insight may be obtained as additional features are seen by focusing on a single reflection in more detail, Figure 4b.

dx.doi.org/10.1021/ic202571d | Inorg. Chem. 2012, 51, 3648−3655

Table 1. Elemental Analysis Mass Fractions in Percent with Calculated Values in Parentheses and Proposed Chemical Formulas

x	*y*	K	Ni	Co	Fe	Cr	C	N	H	O
	0.0	2.98 (3.29)		12.54 (19.85)	2.04 (0)	13.01 (13.14)	18.02 (18.21)	20.78 (21.23)	2.73 (2.72)	21.84 (21.56)
proposed chemical formula: $K_{0.25}Co_{1.00}[Cr(CN)_6]_{0.75}[(H_2O)_6]_{0.25}\cdot 2.5H_2O$							shorthand: CoCr		formula mass: 296.84 g/mol	
	0.2	3.07 (3.29)		17.98 (19.81)	5.79 (2.82)	10.76 (10.49)	18.14 (18.17)	20.86 (21.19)	2.67 (2.71)	21.36 (21.52)
proposed chemical formula: $K_{0.25}Co_{1.00}[Fe(CN)_6]_{0.15}[Cr(CN)_6]_{0.60}[(H_2O)_6]_{0.25}\cdot 2.5H_2O$							shorthand: $CoFe_{0.2}Cr_{0.8}$		formula mass: 297.42 g/mol	
	0.4	3.12 (3.28)		18.80 (19.78)	6.47 (5.62)	7.98 (7.85)	18.06 (18.14)	20.92 (21.15)	2.59 (2.71)	20.72 (21.48)
proposed chemical formula: $K_{0.25}Co_{1.00}[Fe(CN)_6]_{0.30}[Cr(CN)_6]_{0.45}[(H_2O)_6]_{0.25}\cdot 2.5H_2O$							shorthand: $CoFe_{0.4}Cr_{0.6}$		formula mass: 298.00 g/mol	
	0.6	3.36 (3.27)		19.36 (19.74)	9.94 (8.42)	5.26 (5.22)	18.04 (18.10)	20.85 (21.11)	2.74 (2.70)	21.92 (21.43)
proposed chemical formula: $K_{0.25}Co_{1.00}[Fe(CN)_6]_{0.45}[Cr(CN)_6]_{0.30}[(H_2O)_6]_{0.25}\cdot 2.5H_2O$							shorthand: $CoFe_{0.6}Cr_{0.4}$		formula mass: 298.58 g/mol	
	0.8	3.33 (3.27)		19.04 (19.70)	11.77 (11.20)	2.69 (2.61)	17.98 (18.07)	20.89 (21.07)	2.76 (2.70)	22.08 (21.40)
proposed chemical formula: $K_{0.25}Co_{1.00}[Fe(CN)_6]_{0.60}[Cr(CN)_6]_{0.15}[(H_2O)_6]_{0.25}\cdot 2.5H_2O$							shorthand: $CoFe_{0.8}Cr_{0.2}$		formula mass: 299.15 g/mol	
1.0	1.0	3.14 (3.26)		18.92 (19.66)	13.41 (13.97)		17.97 (18.03)	20.73 (21.03)	2.65 (2.69)	21.44 (21.35)
proposed chemical formula: $K_{0.25}Co_{1.00}[Fe(CN)_6]_{0.75}[(H_2O)_6]_{0.25}\cdot 2.5H_2O$							shorthand: CoFe		formula mass: 299.73 g/mol	
0.	---	3.86 (3.26)	3.91 (3.92)	15.22 (15.73)	13.72 (13.98)		18.04 (18.04)	20.81 (21.03)	2.51 (2.69)	20.08 (21.35)
proposed chemical formula: $K_{0.25}Ni_{0.20}Co_{0.80}[Fe(CN)_6]_{0.75}[(H_2O)_6]_{0.25}\cdot 2.5H_2O$							shorthand: $Ni_{0.2}Co_{0.8}Fe$		formula mass: 299.68 g/mol	
0.6		4.29 (3.26)	8.35 (7.84)	12.33 (11.8)	14.93 (13.98)		18.03 (18.04)	20.79 (21.04)	2.58 (2.69)	20.64 (21.36)
proposed chemical formula: $K_{0.25}Ni_{0.40}Co_{0.60}[Fe(CN)_6]_{0.75}[(H_2O)_6]_{0.25}\cdot 2.5H_2O$							shorthand: $Ni_{0.4}Co_{0.6}Fe$		formula mass: 299.64 g/mol	
0.4		3.86 (3.26)	11.94 (11.75)	7.94 (7.87)	14.58 (13.98)		17.98 (18.04)	20.76 (21.04)	2.57 (2.69)	20.56 (21.36)
proposed chemical formula: $K_{0.25}Ni_{0.60}Co_{0.40}[Fe(CN)_6]_{0.75}[(H_2O)_6]_{0.25}\cdot 2.5H_2O$							shorthand: $Ni_{0.6}Co_{0.4}Fe$		formula mass: 299.59 g/mol	
0.2		3.38 (3.26)	17.00 (15.68)	4.14 (3.93)	15.46 (13.98)		18.01 (18.04)	20.72 (21.04)	2.73 (2.69)	21.84 (21.36)
proposed chemical formula: $K_{0.25}Ni_{0.80}Co_{0.20}[Fe(CN)_6]_{0.75}[(H_2O)_6]_{0.25}\cdot 2.5H_2O$							shorthand: $Ni_{0.8}Co_{0.2}Fe$		formula mass: 299.54 g/mol	
0.0		2.60 (3.26)	18.38 (19.60)		12.98 (13.98)		18.00 (18.05)	20.74 (21.05)	2.76 (2.69)	22.08 (21.37)
proposed chemical formula: $K_{0.25}Ni_{1.00}[Fe(CN)_6]_{0.75}[(H_2O)_6]_{0.25}\cdot 2.5H_2O$							shorthand: NiFe		formula mass: 299.49 g/mol	

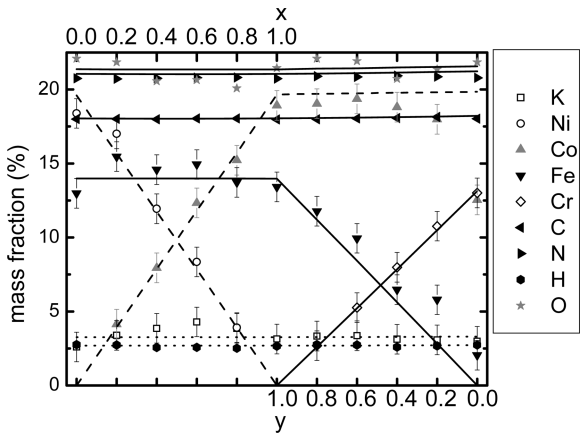

Figure 2. Mass fractions of elements. Experimentally obtained values are shown as data points, while proposed values are shown as lines. Uncertainty bars are derived from measured machine uncertainties, and when not visible they are smaller than the data marker.

The evolution of the structure with nickel substitution is similar to previously reported bistable $Ni_{1-x}Co_xFe$, with a monotonic interpolation between Ni−Fe and Co−Fe structures and a widening line with decreasing x due to smaller particle size.[22] On the other hand, the substitution of chromium for iron in Co−Fe has a decidedly different effect. The evolution of $CoFe_yCr_{1-y}$ diffractograms as a function of y shows nonlinear, nonmonotonic behavior with the smallest lattice constant and broadest line coming from $CoFe_{0.6}Cr_{0.4}$.

D. Infrared Spectroscopy. As an additional probe of the oxidation states of the compounds and how they change because of CTIST, temperature-dependent infrared spectroscopy was performed. Specifically, absorption due to cyanide stretches was observed for all compounds, Figure 5, and the structure of the cyanide stretches is due to the local environment of the cyanide. The CN absorption line splits depending upon the valence of the hexacyano ion, and additional structure of the line occurs due to changes in the

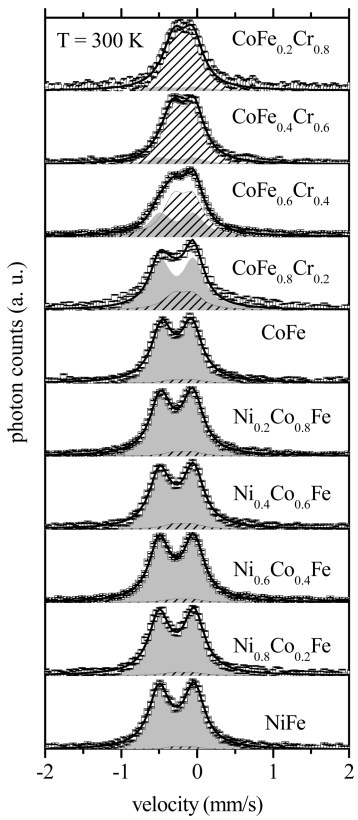

Figure 3. Mössbauer Spectroscopy. Absorption spectra of ^{57}Fe Mossbauer at T = 300 K are shown (□) with a fit (—) that includes Fe^{3+} (gray) and Fe^{2+} (stripes). Uncertainty bars are statistical, representing one standard deviation, and when not visible, they are smaller than the data marker.

binding at the nitrogen site. Because shifts due to the second order effect of the M1 metal ions are small compared to line widths, such effects are integrated out, and only changes due to M2 metal ions are considered. The result of fitting the data to this model is summarized in Table 3. As a starting point, the

dx.doi.org/10.1021/ic202571d | Inorg. Chem. 2012, 51, 3648−3655

Table 2. Parameters from fitting Mössbauer Spectra in Figure 3[a]

sample			Fe^{2+}		Fe^{3+}	
shorthand	x	y	QS	%	QS	%
$CoFe_{0.2}Cr_{0.8}$		0.2	0.12	94	0.22	6
$CoFe_{0.4}Cr_{0.6}$		0.4	0.14	89	0.22	11
$CoFe_{0.6}Cr_{0.4}$		0.6	0.13	62	0.22	38
$CoFe_{0.8}Cr_{0.2}$		0.8	0.12	22	0.22	78
CoFe	1.0	1.0	0.12	5	0.20	95
$Co_{0.8}Ni_{0.2}Fe$	0.8		0.12	6	0.21	94
$Co_{0.6}Ni_{0.4}Fe$	0.6		0.12	7	0.22	93
$Co_{0.4}Ni_{0.6}Fe$	0.4		0.12	5	0.23	95
$Co_{0.2}Ni_{0.8}Fe$	0.2		0.12	7	0.23	96
NiFe	0.0		0.12	3	0.23	97

[a]The line-widths, Fe^{2+} isomer shifts, and Fe^{3+} isomer shifts were fit globally across all spectra to give 0.33 mm/s, −0.181 mm/s, and −0.27 mm/s, respectively.

pure CoFe material shows both M_2^{2+}−CN− and M_2^{3+}−CN− peaks at room temperature, with all M_2^{3+}−CN− species transforming into M_2^{2+}−CN− at low temperatures. As expected, pure NiFe and CoCr materials are dominated by M_2^{3+}−CN− stretches, with no change as samples are cooled to low temperatures. In the mixed regime for $Ni_{1-x}Co_xFe$, only part of the material shows a transformation, and in $x = 0.2$, $Ni_{0.8}Co_{0.2}Fe$ data, no clear change in peaks as a function of temperature is observed despite having an appreciable fraction of cobalt−iron pairs. Similarly, mixed $CoFe_yCr_{1-y}$ materials do not show any change by $y = 0.2$ substitution levels; however, a clear difference from nickel substitution is that for $y < 1$, M_2^{2+}−CN− species are stabilized at the expense of M_2^{3+}−CN−.

E. Magnetization. The temperature dependences of the dc magnetizations below 30 K are shown in Figure 6. Quenched states are attained by insertion from 300 K to the 100 K magnetometer cryostat. Ground states are reached after warming quenched states to 200 K, and photoinduced states were achieved by photoirradiation at 5 K for 5 h with visible light. Clear changes with photoirradiation and quenching are observed for $x > 0.5$ and $y > 0.5$. The ability to thermally quench potassium cobalt hexacyanoferrate samples is consistent with the pure material.[37] The magnetic ordering temperature, T_C, of each sample is extracted by the onset of a large change of the slope in the magnetization, Table 4. The ordering temperatures of the ternary transition metal samples are seen to interpolate between the binary compounds, although not in a linear way.

IV. DISCUSSION

Substitution of solids away from pure photomagnetic Co−Fe powder has been performed in a systematic way to simulate the potential mixing at interfaces present in high temperature photomagnetic heterostructures based upon Co−Fe and Ni−Cr Prussian blue analogues. It is clear from the experimental results that there is a modification of the Co−Fe containing solid solutions beyond simple percentwise substitutions. In the following, results from the different experimental probes will be considered in concert. Specifically, the nonmonotonic changes in the lattice constant, the low-temperature magnetization, and the Fe^{3+} to Fe^{2+} ratio in the samples are expounded upon.

While ostensibly distinct, the parameters measured in the different experiments are related, and an emergent model should be made self-consistent. To begin with, elemental analysis has established reasonable chemical formulas for the measured compounds and puts a bound on acceptable values for the constituent elements. The Mossbauer measurements make precedented distinction between trivalent and divalent iron in the sample, based upon the different electric field gradients at the nucleus.

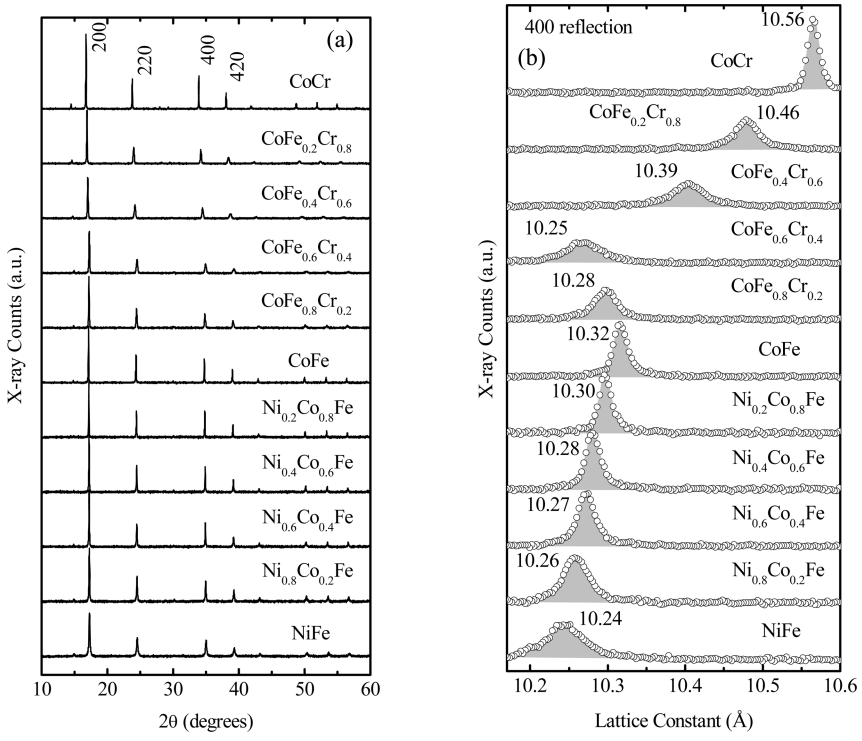

Figure 4. X-ray Diffraction. Powder diffractograms at $T = 300$ K are shown over (a) all angles studied and for (b) the 400 reflection with peak positions annotated. Uncertainty bars are statistical, representing one standard deviation, and when not visible, they are smaller than the data marker.

dx.doi.org/10.1021/ic202571d | Inorg. Chem. 2012, 51, 3648−3655

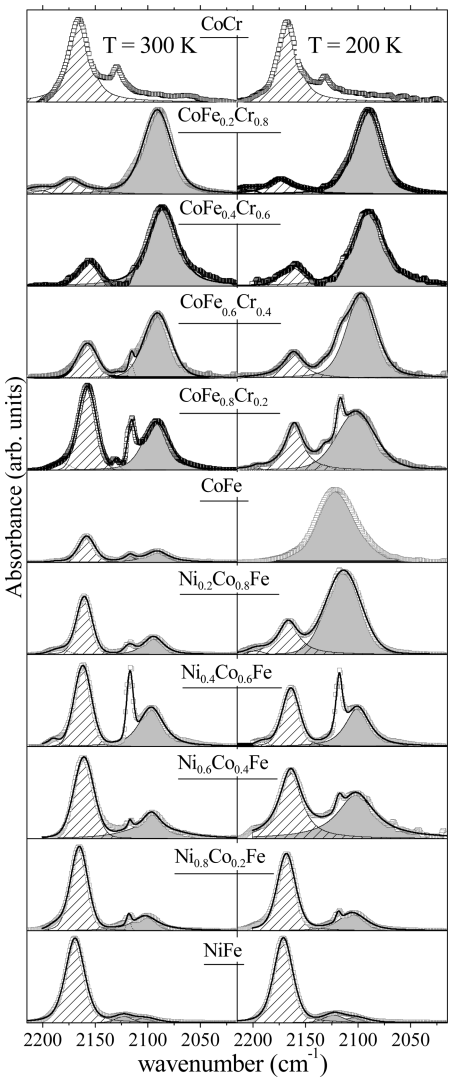

Figure 5. Infrared spectroscopy. Absorption spectra of FT-IR at T = 300 K (a) and T = 200 K (b) are shown (□) with a fit (—) that includes an M_2^{3+}–CN– peak (stripes) and an M_2^{2+}–CN– peak (gray). Anomalously sharp peaks are attributed to precursor contamination of the slides and have no temperature dependence. Uncertainty bars are statistical, representing one standard deviation, and when not visible, they are smaller than the data marker.

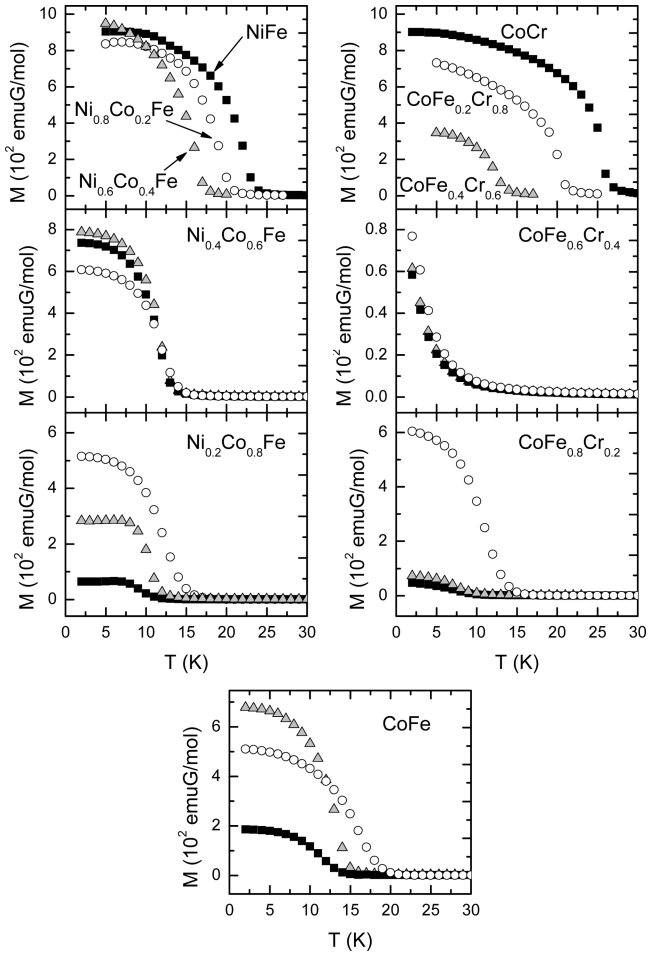

Figure 6. Low-temperature magnetization. The molar magnetization in 10 G after field-cooling with the quenched (▲), photoinduced (○), and ground state (■) shown for x > 0.5 and y > 0.5 materials and the robust ground state shown for x < 0.5 and y < 0.5. Uncertainty bars are derived from fits to voltage profiles of the magnetometer and represent one standard deviation, and when not visible they are smaller than the data marker. Molecular formulas used for normalization are taken from Table 1. A conversion to Bohr magnetons (μ_B) is straightforward using 1 $N\mu_B$ = 5585 emuG/mol, where N is Avogadro's number.

The observation of ferrocyanide in the sample must be considered in the chemical formula. The formulas for the $Ni_xCo_{1-x}Fe$ series are more resilient, as any Fe^{2+} content at room temperature is so small as to be similar to the level of the

Table 3. Relative Areas of Peaks Associated with Trivalent Hexacyanometalates and Divalent Hexacyanometalates from Fitting Infrared Spectra in Figure 4

sample			T = 200 K				T = 300 K			
			M_2^{2+}–CN–		M_2^{3+}–CN–		M_2^{2+}–CN–		M_2^{3+}–CN–	
shorthand	x	y	area	position	area	position	area	position	area	position
CoCr		0.0			1.00	2166.9			1.00	2165.1
$CoFe_{0.2}Cr_{0.8}$		0.2	0.83	2091.0	0.03	2173.8	0.83	2091.0	0.03	2173.8
$CoFe_{0.4}Cr_{0.6}$		0.4	0.88	2090.3	0.06	2162.7	0.88	2085.9	0.06	2156.9
$CoFe_{0.6}Cr_{0.4}$		0.6	0.80	2097.0	0.20	2161.5	0.52	2091.0	0.20	2157.5
$CoFe_{0.8}Cr_{0.2}$		0.8	0.62	2099.7	0.38	2161.0	0.45	2092.1	0.45	2157.8
CoFe	1.0	1.0	1.00	2122.7			0.10	2091.0	0.14	2158.3
$Co_{0.8}Ni_{0.2}Fe$	0.8		0.75	2113.8	0.25	2166.5	0.12	2094.7	0.24	2160.4
$Co_{0.6}Ni_{0.4}Fe$	0.6		0.53	2100.4	0.47	2163.9	0.42	2096.8	0.46	2161.8
$Co_{0.4}Ni_{0.6}Fe$	0.4		0.40	2101.9	0.46	2164.1	0.25	2096.5	0.38	2160.9
$Co_{0.2}Ni_{0.8}Fe$	0.2		0.27	2105.5	0.73	2168.2	0.25	2102.4	0.69	2165.2
NiFe	0.0		0.07	2105.5	0.93	2171.0	0.05	2102.5	0.99	2169.3

dx.doi.org/10.1021/ic202571d | Inorg. Chem. 2012, 51, 3648–3655

Table 4. Magnetic Ordering Temperatures of the Solid Solutions in Different States

sample			T_C [K]		
shorthand	x	y	photo	quench	ground
CoCr		0.0	26.6	26.6	26.6
$CoFe_{0.2}Cr_{0.8}$		0.2	21.3	21.3	21.3
$CoFe_{0.4}Cr_{0.6}$		0.4	13.8	13.8	13.8
$CoFe_{0.6}Cr_{0.4}$		0.6	<2 K	<2 K	<2 K
$CoFe_{0.8}Cr_{0.2}$		0.8	13.9	9.3	9.2
CoFe	1.0	1.0	18.8	14.5	13.9
$Co_{0.8}Ni_{0.2}Fe$	0.8		15.2	11.7	11.6
$Co_{0.6}Ni_{0.4}Fe$	0.6		14.2	13.3	13.3
$Co_{0.4}Ni_{0.6}Fe$	0.4		17.3	17.3	17.3
$Co_{0.2}Ni_{0.8}Fe$	0.2		20.7	20.7	20.7
NiFe	0.0		23.6	23.6	23.6

uncertainties and nearly constant for different values of x. On the other hand, Fe^{2+} content is nonperturbative in the $CoFe_yCr_{1-y}$ series and must be reflected upon in detail. On the basis of only the Mossbauer measurements, it is possible that the iron is being reduced independently ($Co^{3+}/Fe^{2+} \equiv 0$) or that the iron reduction takes place concurrently with an offsetting cobalt oxidation ($Co^{3+}/Fe^{2+} \equiv 1$), and these two models were compared using least-squares fits to elemental analysis, where residuals were inversely weighted according to experimental uncertainty and the iron residual was also softened by a factor of 10 because larger scatter was observed in these data. For fitting, C and N fractions were fixed to each other and further constrained to be 6 times in number compared to the sum of Fe and Cr atoms, while the number of O atoms was set to be half the number of H atoms. Normalizing to one Co atom, and taking iron oxidation states directly from Mossbauer, four fitting parameters were utilized: the number of K atoms (K), the number of H atoms (H), the ratio of Fe and Cr to Co (M2/M1), and the ratio of Fe to Cr (y_{fit}). Results of fits are shown in Table 5 and Figure 7.

Table 5. Least Squares Fits Parameters Comparing Charge-Balancing Models for $CoFe_yCr_{1-y}$

y	Co^{3+}/Fe^{2+}	K	H	M2/M1	y_{fit}
0.2	0	0.33	8.00	0.75	0.13
	1	0.32	8.44	0.77	0.20
0.4	0	0.32	7.29	0.71	0.31
	1	0.30	8.22	0.77	0.40
0.6	0	0.30	7.26	0.69	0.51
	1	0.27	8.32	0.76	0.61
0.8	0	0.29	7.74	0.72	0.77
	1	0.27	8.34	0.76	0.80

The lattice constants are seen to change as the chemical formula is changed. Interestingly, the chromium substitution gives rise to first a decrease then an increase in the volume of the crystallographic unit. This behavior may be reproduced by considering the relative proportion of differently structured species in each compound and, specifically, the presence of Co^{3+}. Values of 10.56 Å for Co−Cr and 10.24 Å for Ni−Fe species are taken from the $y = 0$ and $x = 0$ compounds, respectively. For the Co−Fe constituents, room-temperature EXAFS has previously been reported on these compounds that shows Fe−N distances to be around 3.05 Å with variations on the order of 0.01 Å for compounds with different Fe^{2+}/Fe^{3+}

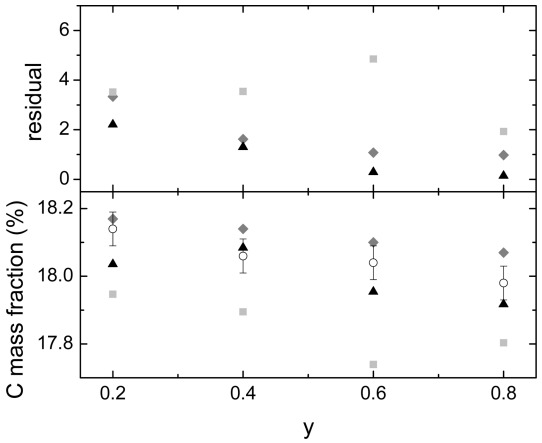

Figure 7. Comparison of charge balancing models for $CoFe_yCr_{1-y}$. The residuals from models for the chemical formula (Table 5) that balance charge while $Co^{3+}/Fe^{2+} \equiv 0$ (■), $Co^{3+}/Fe^{2+} \equiv 1$ (▲), and the global fit previously presented in Table 1 that is valid when $Co^{3+}/Fe^{2+} \equiv 1$ (♦). The carbon mass fraction is also illustrative of the goodness of fit, and experimental data (○) are compared to the $Co^{3+}/Fe^{2+} \equiv 0$ model (■), $Co^{3+}/Fe^{2+} \equiv 1$ (▲), and the global fit previously presented in Table 1 that is valid when $Co^{3+}/Fe^{2+} \equiv 1$ (♦).

ratios, while the Co−N distance is an order of magnitude greater in sensitivity to oxidation state with the Co^{3+}−N distance nominally 1.90 Å, as taken from a Co^{3+} rich material, and the Co^{2+}−N distance nominally 2.11 Å, as taken from a Co^{2+} rich material.[38] Simple linear interpolation between constituents reproduces the observations well for most data but agrees less for materials that have a high degree of strain, Figure 8. It is worth noting that unaccounted Co^{2+} in the

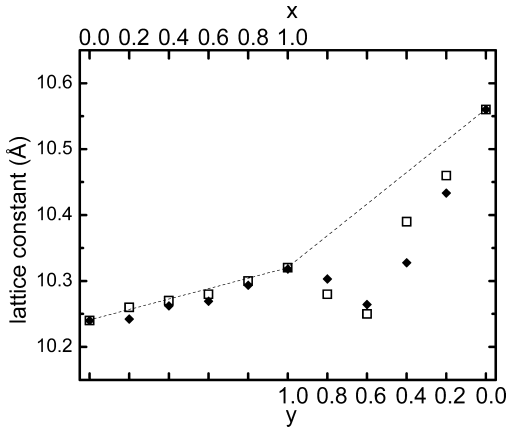

Figure 8. Lattice constants. The trends observed in experimentally obtained values (□) can be reproduced by averaging the lattice constants of the constituent binary transition metal materials (♦), and an interpolation assuming all M1 ions are divalent is also shown (dashed line). Uncertainty bars are standard errors from fits to peak positions, and when not visible they are smaller than the data marker.

$y = 0.4$ and $y = 0.2$ samples may also be attributing to the differences in lattice constants from averaged values, but the chemical analysis suggests such an effect should be small and that perturbations are most likely due to nonlinearity from strain. Furthermore, these diffraction data support the solid solution character of the samples due to the single unit cell constant for each sample, in contrast with analogous heterostructures that have distinct crystallographic phases.[14,39]

dx.doi.org/10.1021/ic202571d | Inorg. Chem. 2012, 51, 3648−3655

The low-temperature magnetization shows similarities with previous work on photomagnetic solid solutions[21,22] but also has new features. The pure Co−Fe material shows the well documented increase in ordering temperature and magnetization with photoirradiation, while quenching only subtly increases the ordering temperature while increasing the magnetization, and the same trend is seen in samples with substitution that shows photomagnetic effects. The $CoFe_{0.8}Cr_{0.2}$ sample has little magnetism present in quenched and ground states but shows a large effect with photoirradiation, while the $Ni_{0.2}Co_{0.8}Fe$ sample has a similar magnitude photoeffect, with more of a propensity for trapping high spin states with thermal quenching. For the $CoFe_{0.6}Cr_{0.4}$ material, changes can be seen with irradiation and quenching, but there is not sufficient cooperativity to support magnetic ordering, likely due to the dominance of diamagnetic Fe^{2+} in this sample. The $K_{0.25}Ni_{0.40}Co_{0.60}[Fe(CN)_6]_{0.75}[(H_2O)_6]_{0.25}\cdot 2.5H_2O$, $Ni_{0.4}Co_{0.6}Fe$ sample is highly interesting, as a similar material, $Na_{0.33}Co^{2+}_{0.66}Ni^{2+}_{0.34}[Fe^{3+}(CN)_6]_{0.67}[Fe^{2+}(CN)_6]_{0.08}\cdot 4.6H_2O$, was shown to decrease magnetization with photoirradiation.[21] The photoinduced decrease is reproduced; however, quenching the sample actually *increases* the magnetization. These results suggest that quenched versus ground states of these samples change the total amount of magnetic material without strongly affecting the microstructure of the materials, while photoirradiation does.

By combining the results of Mössbauer and infrared spectroscopy experiments, infrared absorptivity coefficients of the cyanide stretches and the high spin iron fraction of the different sample may be extracted. For nickel substitution, the relative ratio of divalent iron to trivalent iron coordinated cyanide infrared absorptivities was found to be nearly 10:1. For analyzing infrared spectra of chromium substitution, this same ratio could be kept for iron coefficients, but chromium coordinated cyanides showed decreasing absorption coefficients with increasing chromium in the lattice. Namely, the ratio of absorption coefficients for divalent iron coordinated cyanides to chromium coordinated cyanides went from 1/2 for $CoFe_{0.8}Cr_{0.2}$ to 1/3 for $CoFe_{0.6}Cr_{0.4}$ to 1/10 for $CoFe_{0.4}Cr_{0.6}$, and finally less than 1/20 for $CoFe_{0.2}Cr_{0.8}$. The ratio of Fe^{3+} to Fe^{2+} based upon the spectroscopic experiments is shown in Figure 9. The

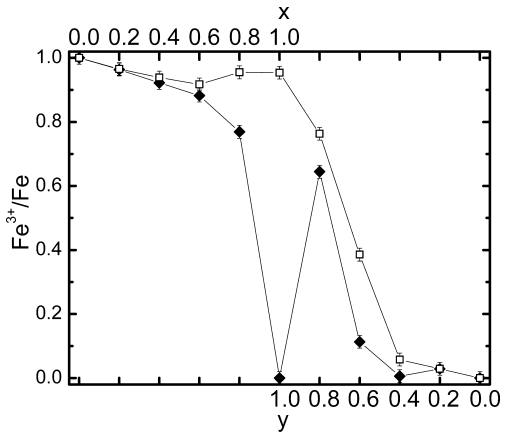

Figure 9. High spin fraction changes with chemical composition. High spin fraction is shown for 300 K (□) and 200 K (♦). Uncertainty bars are standard errors from fitting the experimental data.

underlying reason for the loss of bistability is likely to be due to the rigid bonds of the materials that are not photomagnetic that make the cooperative photoinduced magnetism process unfavorable. The Ni−Fe lattice constant is nearly the same as the high spin Co−Fe lattice constant, while the Co−Cr lattice constant may be so much larger that Co−Fe bonds in the same lattice stabilize in the shorter, low spin configuration.

V. CONCLUSIONS

We have demonstrated that bistable Co−Fe persists for low-level substitution of Cr for Fe and Ni for Co and is destroyed at high substitution levels. Furthermore, Cr substituted for Fe in Co−Fe stabilizes toward diamagnetic Co/Fe, while Ni substitution for Co stabilizes toward magnetic Co/Fe. As such, when attempting to synthesize microstructured and nanostructured "meta-materials" that contain the photoactive Co−Fe constituent, care must be taken to preserve sufficiently chemically pure regions in the solid if photoeffects due to Co−Fe are to be observed.

AUTHOR INFORMATION

Corresponding Author

*E-mail: einaga@chem.keio.ac.jp and daniel@pajerowski.com.

Notes

The authors declare no competing financial interest.

ACKNOWLEDGMENTS

This work was supported by a Grant-in-Aid for Scientific Research on Innovative Areas ("Coordination Programming" Area 2107, Grant No. 22108530) from MEXT, Japan, and D.M.P. acknowledges support from the East Asia and Pacific Summer Institutes program of the National Science Foundation.

REFERENCES

(1) Gütlich, P.; Garcia, Y.; Woike, T. *Coord. Chem. Rev.* **2001**, *219−221*, 839.
(2) Varret, F.; Boukheddaden, K.; Codjovi, E.; Goujon, A. *Hyperfine Interact.* **2005**, *65*, 37.
(3) Einaga, Y. *J. Photochem. Photobiol. C: Photochem. Rev.* **2006**, *7*, 69.
(4) Pejaković, D. A.; Kitamura, C.; Miller, J. S.; Epstein, A. J. *Phys. Rev. Lett.* **2002**, *88*, 057202.
(5) Yoo, J.-W.; Edelstein, R.; Lincoln, D.; Raju, N.; Xia, C.; Pokhodnya, K.; Miller, J.; Epstein, A. *Phys. Rev. Lett.* **2006**, *97*, 247205.
(6) Yoo, J.-W.; Edelstein, R.; Lincoln, D.; Raju, N.; Epstein, A. *Phys. Rev. Lett.* **2007**, *99*, 157205.
(7) Gütlich, P.; Goodwin, H. A. *Spin Crossover in Transition Metal Compounds I, II, III*; Springer: Berlin, 2004.
(8) Bousseksou, A.; Molnár, G.; Real, J. A.; Tanaka, K. *Coord. Chem. Rev.* **2007**, *251*, 1822.
(9) Ohkoshi, S.; Hashimoto, K. *J. Photochem. Photobiol. C: Photochem. Rev.* **2001**, *2*, 71.
(10) Shimamoto, N.; Ohkoshi, S.-i.; Sato, O.; Hashimoto, K. *Inorg. Chem.* **2002**, *41*, 678.
(11) Escax, V.; Bleuzen, A.; Cartier dit Moulin, C.; Villain, F.; Goujon, A.; Varret, F.; Verdaguer, M. *J. Am. Chem. Soc.* **2001**, *123*, 12536.
(12) Pajerowski, D. M.; Andrus, M. J.; Gardner, J. E.; Knowles, E. S.; Meisel, M. W.; Talham, D. R. *J. Am. Chem. Soc.* **2010**, *132*, 4058.
(13) Pajerowski, D. M.; Gardner, J. E.; Franz, F. A.; Andrus, M. J.; Dumont, M. F.; Knowles, E. S.; Meisel, M. W.; Talham, D. R. *Chem. Mater.* **2011**, *23*, 3045.
(14) Dumont, M. F.; Knowles, E. S.; Guiet, A.; Pajerowski, D. M.; Gomez, A.; Kycia, S. W.; Meisel, M. W.; Talham, D. R. *Inorg. Chem.* **2011**, *50*, 4295.
(15) Verdaguer, M.; Girolami, G. S. In *Magnetism - Molecules to Materials V*; Miller, J. S., Drillon, M., Eds.; Wiley-VCH: Weinheim, Germany, 2005; Vol. 5, p 283.

(16) Buser, H. J.; Schwarzenbach, D.; Petter, W.; Ludi, A. *Inorg. Chem.* **1977**, *16*, 2704.
(17) Gadet, V.; Mallah, T.; Castro, I.; Verdaguer, M.; Veillet, P. *J. Am. Chem. Soc.* **1992**, *114*, 9213.
(18) Sato, O.; Iyoda, T.; Fujishima, A.; Hashimoto, K. *Science* **1996**, *272*, 704.
(19) Sato, O.; Einaga, Y.; Fujishima, A.; Hashimoto, K. *Inorg. Chem.* **1999**, *38*, 4405.
(20) Pajerowski, D. M. Ph. D. Dissertation. University of Florida, Gainesville, FL, 2010.
(21) Cafun, J.-D.; Londinière, L.; Rivière, E.; Bleuzen, A. *Inorg. Chim. Acta* **2008**, *361*, 3555.
(22) Pajerowski, D. M.; Gardner, J. E.; Talham, D. R.; Meisel, M. W. *J. Am. Chem. Soc.* **2009**, *131*, 12927.
(23) Kumar, A.; Yusuf, S. M.; Keller, L.; Yahkmi, J. V.; Srivastava, J. K.; Paulose, P. L. *Phys. Rev. B* **2007**, *75*, 224419.
(24) Kumar, A.; Yusuf, S. M. *Physica B* **2005**, *362*, 278.
(25) Ohkoshi, S.; Iyoda, T.; Fujishima, A.; Hashimoto, K. *Phys. Rev. B* **1997**, *56*, 11642.
(26) Ohkoshi, S.-i; Sato, O.; Iyoda, T.; Fujishima, A.; Hashimoto, K. *Inorg. Chem.* **1997**, *36*, 268.
(27) Ohkoshi, S.-i.; Hashimoto, K. *Phys. Rev. B* **1999**, *60*, 12820.
(28) Widmann, A.; Kahlert, H.; Petrovic-Prelevic, I.; Wulff, H.; Yakhmi, J. V.; Bagkar, N.; Scholz, F. *Inorg. Chem.* **2002**, *41*, 5706.
(29) Bagkar, N.; Widmann, A.; Kahlert, H.; Ravikumar, G.; Yusuf, S. M.; Scholz, F.; Yakhmi, J. V. *Philos. Mag.* **2005**, *85*, 3659.
(30) Widmann, A.; Kahlert, H.; Wulff, H.; Scholz, F. *J. Solid State Electrochem.* **2005**, *9*, 380.
(31) Schwudke, D.; Stösser, R.; Scholz, F. *Electrochem. Commun.* **2000**, *2*, 301.
(32) Lummen, T. T. A.; Gengler, R. Y. N.; Rudolf, P.; Lusitani, F.; Vertelman, E. J. M.; van Koningsbruggen, P. J.; Knupfer, M.; Molodtsova, O.; Pireaux, J.-J.; van Loosdrecht, P. H. M. *J. Phys. Chem. C* **2008**, *112*, 14158.
(33) Certain commercial equipment, instruments, or materials are identified in this paper to foster understanding. Such identification does not imply recommendation or endorsement by the National Institute of Standards and Technology, nor does it imply that the materials or equipment identified are necessarily the best available for the purpose.
(34) Ng, C. W.; Ding, J.; Gan, L. M. *J. Solid State Chem.* **2001**, *156*, 400.
(35) Ng, C. W.; Ding, J.; Shi, Y.; Gan, L. M. *J. Phys. Chem. Solids* **2001**, *62*, 767.
(36) Ding, J.; Ng, C. W.; Shi, Y. *IEEE Trans. Magn.* **2001**, *37*, 2938.
(37) Park, J.-H.; Frye, F.; Anderson, N. E.; Pajerowski, D. M.; Huh, Y. D.; Talham, D. R.; Meisel, M. W. *J. Magn. Magn. Mater.* **2007**, *310*, 1458.
(38) Yokoyama, T.; Ohta, T.; Sato, O.; Hashimoto, K. *Phys. Rev. B* **1998**, *58*, 8257.
(39) Presle, M.; Lemainque, J.; Guigner, J.-M.; Larquet, E.; Maurin, I.; Boilot, J.-P.; Gacoin, T. *New J. Chem.* **2011**, *35*, 1296.